Title

Expression of an active Gαs mutant in skeletal stem cells is sufficient and necessary for fibrous dysplasia initiation and maintenance

Journal

Proceedings of the National Academy of Sciences of the United States of America, 115(3)

ISSN

0027-8424

Authors

Zhao, Xuefeng

Deng, Peng

Iglesias-Bartolome, Ramiro

et al.

Publication Date

2018-01-16

DOI

10.1073/pnas.1713710115

Expression of an active $G\alpha_s$ mutant in skeletal stem cells is sufficient and necessary for fibrous dysplasia initiation and maintenance

Xuefeng Zhao[a,b], Peng Deng[a], Ramiro Iglesias-Bartolome[c], Panomwat Amornphimoltham[b,d], Dana J. Steffen[b,e], Yunyun Jin[f,g], Alfredo A. Molinolo[b], Luis Fernandez de Castro[h], Diana Ovejero[h], Quan Yuan[a], Qianming Chen[a], Xianglong Han[a], Ding Bai[a], Susan S. Taylor[e,i], Yingzi Yang[f], Michael T. Collins[h], and J. Silvio Gutkind[b,e,1]

[a]State Key Laboratory of Oral Diseases, National Clinical Research Center for Oral Diseases, West China Hospital of Stomatology, Sichuan University, Chengdu, 610041, China; [b]Moores Cancer Center, University of California, San Diego, La Jolla, CA 92093; [c]National Cancer Institute, National Institutes of Health, Bethesda, MD 20892; [d]International College of Dentistry, Walailak University, Nakhon Si Thammarat, 80161, Thailand; [e]Department of Pharmacology, University of California, San Diego, La Jolla, CA 92093; [f]Department of Developmental Biology, Harvard School of Dental Medicine, Boston, MA 02115; [g]Institute of Biomedical Sciences and School of Life Sciences, East China Normal University, Shanghai, 200241, China; [h]Section on Skeletal Disorders and Mineral Homeostasis, National Institute of Dental and Craniofacial Research, National Institutes of Health, Bethesda, MD 20892; and [i]Department of Chemistry and Biochemistry, University of California, San Diego, La Jolla, CA 92093

Edited by John T. Potts, Massachusetts General Hospital, Charlestown, MA, and approved December 6, 2017 (received for review August 2, 2017)

Fibrous dysplasia (FD) is a disease caused by postzygotic activating mutations of *GNAS* (R201C and R201H) that encode the α-subunit of the G_s stimulatory protein. FD is characterized by the development of areas of abnormal fibroosseous tissue in the bones, resulting in skeletal deformities, fractures, and pain. Despite the well-defined genetic alterations underlying FD, whether *GNAS* activation is sufficient for FD initiation and the molecular and cellular consequences of *GNAS* mutations remains largely unresolved, and there are no currently available targeted therapeutic options for FD. Here, we have developed a conditional tetracycline (Tet)-inducible animal model expressing the $G\alpha_s^{R201C}$ in the skeletal stem cell (SSC) lineage (Tet–$G\alpha_s^{R201C}$/*Prrx1*-Cre/LSL-rtTA-IRES-GFP mice), which develops typical FD bone lesions in both embryos and adult mice in less than 2 weeks following doxycycline (Dox) administration. Conditional $G\alpha_s^{R201C}$ expression promoted PKA activation and proliferation of SSCs along the osteogenic lineage but halted their differentiation to mature osteoblasts. Rather, as is seen clinically, areas of woven bone admixed with fibrous tissue were formed. $G\alpha_s^{R201C}$ caused the concomitant expression of receptor activator of nuclear factor kappa-B ligand (Rankl) that led to marked osteoclastogenesis and bone resorption. $G\alpha_s^{R201C}$ expression ablation by Dox withdrawal resulted in FD-like lesion regression, supporting the rationale for $G\alpha_s$-targeted drugs to attempt FD cure. This model, which develops FD-like lesions that can form rapidly and revert on cessation of mutant $G\alpha_s$ expression, provides an opportunity to identify the molecular mechanism underlying FD initiation and progression and accelerate the development of new treatment options.

GNAS | skeletal stem cell | fibrous dysplasia | mouse models | PKA

Fibrous dysplasia of bone (FD) [Online Mendelian Inheritance in Man (OMIM) 174800] is a skeletal disease that in more severe cases can be quite debilitating, and in the most severe forms, a life-threatening disease. It is caused by early embryonic postzygotic somatic activating mutations of *GNAS* (refSNP rs11554273 and rs121913495). Activating *GNAS* mutations encode the GTPase defective α-subunit of the heterotrimeric G protein G_s (1–3). FD is a disease of postnatal skeletal stem cells (4–7) (SSCs) that arises as a result of stochastic *GNAS* mutations encoding $G\alpha_s^{R201C}$ or $G\alpha_s^{R201H}$, resulting in a somatic mosaic state (1, 8). FD is characterized by the development of areas of fibroosseous tissue in the bones. It can compromise a single bone (monostotic) or more than one (polyostotic). In its more severe form, FD results in frequent bone fractures, deformities, and pain (9). Because $G\alpha_s$ and its linked receptors, collectively known as G protein-coupled receptors (GPCRs), play a central role in endocrine gland function, sporadic, mosaic activating $G\alpha_s$ mutations can also lead to autonomous hormone overproduction in multiple glands, such as the gonads and thyroid, pituitary, and adrenal glands (10). This results in early puberty, hyperthyroidism, excess growth hormone (gigantism or acromegaly), and excess cortisol production (Cushing's syndrome) (11). The presence of $G\alpha_s$-driven endocrinopathies, together with abnormal "café-au-lait" skin macules and bone involvement (FD) are characteristic of McCune-Albright syndrome (MAS) (12).

Although $G\alpha_s$ mutants are tumorigenic in multiple tissues, including pituitary and thyroid glands, and oncogenic in pancreas and colon, among others (13), tissues involved in FD/MAS, including bone, rarely (<1%) undergo malignant transformation (14, 15). Increased levels of cAMP (13) constitute the downstream mediator of the effects of constitutively active $G\alpha_s$ mutants. Despite this well-defined genetic alteration and downstream effects underlying FD/MAS, the molecular and cellular consequences of $G\alpha_s$ activation remain largely unresolved, and there are no currently available targeted therapeutic options for FD (2).

To date, available $G\alpha_s$-expressing mouse models develop variable pathological manifestations, including FD lesions in adulthood after a long latency (more than 1 y of age) (16). This raises the possibility

Significance

We generated a novel conditional inducible mouse model of fibrous dysplasia (FD) by expressing mutant *GNAS* in skeletal stem cells (SSCs) in a temporally controlled and tissue-specific fashion. Typical FD bone lesions developed rapidly in mutant embryos and postnatal mice. *GNAS* promoted PKA activation and proliferation of SSCs along the osteogenic lineage but impaired their differentiation to mature osteoblasts and triggered increased osteoclastogenesis and bone resorption. FD lesions reverted on cessation of *GNAS* expression. Thus, *GNAS* mutation is sufficient and necessary for FD initiation and maintenance. This model provides a valuable opportunity to identify the molecular mechanism underlying FD progression and accelerate the development of more effective treatment options.

Author contributions: X.Z., Q.C., D.B., M.T.C., and J.S.G. designed research; X.Z., P.D., R.I.-B., P.A., D.J.S., Y.J., A.A.M., L.F.d.C., and D.O. performed research; R.I.-B., P.A., S.S.T., and Y.Y. contributed new reagents/analytic tools; X.Z., R.I.-B., P.A., D.J.S., Y.J., A.A.M., L.F.d.C., D.O., Q.Y., Q.C., X.H., S.S.T., M.T.C., and J.S.G. analyzed data; and X.Z., L.F.d.C., Q.C., M.T.C., and J.S.G. wrote the paper.

The authors declare no conflict of interest.

This article is a PNAS Direct Submission.

[1]To whom correspondence should be addressed. Email: sgutkind@ucsd.edu.

This article contains supporting information online at www.pnas.org/lookup/suppl/doi:10.1073/pnas.1713710115/-/DCSupplemental.

that multiple additional events subsequent to $G\alpha_s$ mutant expression and aberrant cell proliferation may contribute to FD, which in turn may need to be targeted for therapeutic intervention in this disease. Indeed, the precise nature of the FD/MAS initiating cells, as well as whether $G\alpha_s$ active mutants are strictly necessary once FD/MAS is established, is at present unknown (16).

We show here that the combinatorial use of Cre-mediated conditional and tetracycline (Tet)-inducible systems resulting in the expression of mutant $G\alpha_s$ in SSCs is sufficient to recapitulate the clinical complexities of FD/MAS in less than 2 wk after mutant $G\alpha_s$ induction. We also observed that reducing $G\alpha_s$ expression by doxycycline (Dox) withdrawal resulted in clinical improvement of the affected mice in 4 mo, supporting the central tenet that stopping the expression or activity of $G\alpha_s$ will halt FD progression and promote the regression of preexisting FD lesions. The use of this genetically defined inducible FD mouse model with a rapid onset of disease progression may provide an opportunity to understand FD development at the molecular and cellular level and accelerate the development and evaluation of new FD treatments.

Results

Development of Conditional and Doxycycline-Inducible Mice Expressing $G\alpha_s^{R201C}$ in Skeletal Stem Cell Lineage Results in FD-Like Lesions. As part of our effort to study how G proteins control stem cell fate and contribute to FD lesion formation, we developed conditional transgenic mice expressing *GNAS*-activating mutants under the control of Tet-responsive elements (Tet-$G\alpha_s^{R201C}$), which was rapidly induced after Dox treatment. We have recently shown that these Tet-$G\alpha_s^{R201C}$ mice, when crossed with cytokeratin 5 promoter (K5rtTA) mice, developed a robust phenotype in a tissue-specific fashion and induced rapid stem cell differentiation (17). Paired-related homeobox 1 (*Prrx1*)-*Cre* mice, expressing *Cre* recombinase under the control of *Prrx1*-derived enhancer, are frequently used to study bone development, as it is expressed in the early limb bud mesenchyme and in a subset of craniofacial mesenchymal cells (18, 19), as well as in postnatal SSCs in limb and craniofacial bones (20, 21). LSL-rtTA-IRES-GFP is known as a "linker" mouse, as it only expresses rtTA and GFP proteins after the expression of *Cre* recombinase that eliminates a *Loxp-STOP-Loxp* (*LSL*) cassette in the *Prrx1*-expressing cells, resulting in conditional and cell type-specific expression of rtTA and GFP simultaneously (22).

To investigate whether expression of $G\alpha_s^{R201C}$ in bone progenitor (stem) cells is sufficient to initiate FD, we crossed Tet-$G\alpha_s^{R201C}$ mice with double transgenic *Prrx1-Cre* and linker mice (Fig. 1*A*). All pups were born healthy with no obvious difference in either size or behavior. Specific expression of $G\alpha_s^{R201C}$ transgene in bone tissues was confirmed by quantitative PCR (qPCR) analysis and Glu-Glu (EE) tag immunoblotting and found associated with phosphorylation of cAMP-responsive element-binding protein (CREB), downstream signaling of $G\alpha_s$ (Fig. 1 *B* and *C*) in mutant ($G\alpha_s^{R201C}$, Tet-$G\alpha_s$/linker/*Prrx1*-Cre) mice. This finding is consistent with the markedly elevated intracellular cyclic adenosine monophosphate (cAMP) and protein kinase A (PKA) phosphorylation observed in Dox-treated $G\alpha_s^{R201C}$ bone marrow stromal cell (BMSC) cultures (Fig. 1 *D* and *E*). Breeding $G\alpha_s^{R201C}$ mice with double-fluorescent Cre reporter mice (*ROSA26 mT/mG*) confirmed the skeletal-specific lineage of the Cre-recombination event in the limbs, showing green Cre activation and red unrecombined tissues in an adult Dox-treated mouse (Fig. 1*F* and Fig. S1*A*). Indeed, we confirmed that $G\alpha s^{R201C}$ is not expressed in other nonosseous tissues, such as muscle and skin. FD-like lesions initiated specifically from growth plates within limb bones in $G\alpha_s^{R201C}$ mice (Fig. 1*F*). These data support the efficient and tissue-specific activation of the $G\alpha_s$ signaling pathway.

$G\alpha_s^{R201C}$ Expression During Embryogenesis Results in FD-Like Lesions. To investigate the early embryogenic mutation events that give rise to FD, we initiated Dox administration to female mice (6 g/kg in the diet) during gestation from embryonic day 4.5 to investigate the effect of $G\alpha_s^{R201C}$ on bone development during embryogenesis. $G\alpha_s^{R201C}$ pups were born following a Mendelian distribution with obviously dysmorphic limbs compared with their littermates (Fig. 2*A*). Whole-mount staining showed clear limb deformity and marked lytic changes along with impaired mineralization in calvarial sutures of the skull (Fig. 2*B*). Histological analysis of forelimbs demonstrated extensive bone deformity of $G\alpha_s^{R201C}$ with predominance of chondroid matrix and reduced endochondral ossification (Fig. 2*C*). In addition, abnormal undermineralized trabeculae embedded within a dense fibrocellular matrix, a distinctive histological feature of FD, were already present at this stage (23). These findings suggest that activating $G\alpha_s$ mutation could initiate FD early lesions during embryonic bone development.

Rapid Onset of FD-Like Lesions in the Postnatal Skeleton of $G\alpha_s^{R201C}$ Mice. In human, FD typically originates during childhood (12). To better assess the postnatal onset and evolution of the FD lesions, mice were treated with Dox (0.05 g/L in drinking water) at the weaning stage (21 d old) and evaluated visually daily for signs of bone lesions. Although we did not observe any significant abnormalities in ion homeostasis, such as blood phosphate, calcium, potassium, and magnesium, within 1 wk of Dox treatment, most limbs of $G\alpha_s^{R201C}$ mice showed progressive swelling and limping behavior, with FD-like lesions starting at the growth plates (Fig. S2). By 2 wk, all limbs of $G\alpha_s^{R201C}$ mice exhibited FD-like lesions, as judged by the visible swelling and confirmation by radiological and histological analyses; littermates appeared normal (Fig. 3 *A* and *B*). X-ray imaging revealed a FD-resembling "ground glass" appearance in limb bones, with distinct hyperostosis and deformation (Fig. 3*C*). Whole-mount skeletal staining revealed expansive bone deformities and undermineralization of the bone lesions, also typical of human FD (Fig. 3*D*). Furthermore, μCT imaging confirmed these lytic changes and revealed spontaneous microfractures in limb bones (Fig. 3*E*). These bone deformities and fractures led to limping behavior found in $G\alpha_s^{R201C}$ mice. Consistent with a common location of FD lesions in humans, defects in calvarial sutures in skull were also observed by μCT imaging (Fig. 3*F*). Analysis of μCT scans of limb bone revealed reduced bone volume, suggesting increased bone resorption (Fig. 3*G*).

After 2 wk of Dox administration, H&E staining revealed marked deformities in limb bones of $G\alpha_s^{R201C}$ mice with diffuse boundaries of cortical, trabecular, and bone marrow compartments. Normal bone structures were substituted by unstructured fibroosseous tissues, composed of immature, undermineralized woven bone, blended into a fibrocellular matrix of collagen (Fig. 4 *A* and *B*), which diminished, or absent hematopoietic and adipose areas of bone marrow, all distinctive features of human FD (Fig. S3*A*) (23–25). The irregular trabecular pattern was reminiscent of the classic "Chinese characters" feature of FD histology (Fig. S3*A*). Sirius red staining showed a widespread disorganized pattern of woven bone and green birefringent collagen-rich fibrosis in $G\alpha_s^{R201C}$ mice as seen under polarized light (Fig. 4 *C* and *D*). As in human FD, lesions did not show signs of malignant transformation. Additionally, consistent with human FD, $G\alpha_s^{R201C}$ mice showed prominent lesional osteoid, in association with severe mineralization defect, as revealed by Toluidine Blue (Fig. 4*E*) and von Kossa staining (Fig. 4*F*) of undecalcified in polymethyl methacrylate (PMMA)-embedded limb sections. Histomorphometric analysis of these areas demonstrated elevated numbers of osteoblasts and osteoclasts, and a marked increase in osteoid volume compared with control mice (Fig. 4*G*), suggesting increased bone remodeling and defective mineralization. These ectopic intracortical remodeling sites mimic the tunneling resorption pattern in the bones found in human FD and hyperparathyroidism, to which FD is related pathophysiologically ($G\alpha_s$-stimulated cAMP signaling by excess PTH) (2, 26). In conclusion, $G\alpha_s^{R201C}$ mice develop classical histological features of FD lesions.

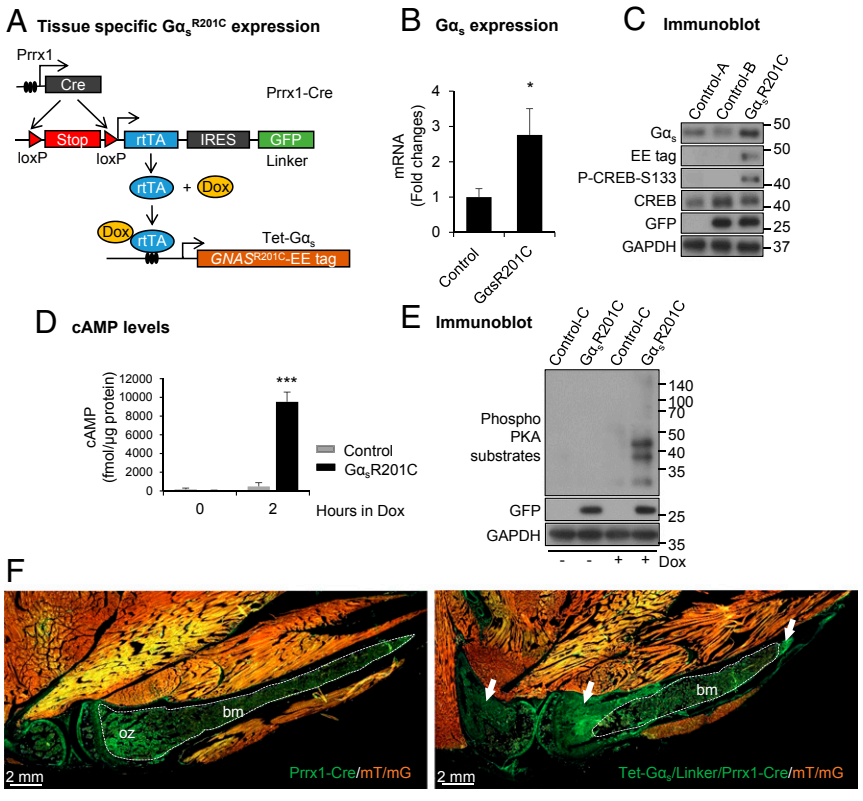

Fig. 1. Generation of the transgenic mouse model of fibrous dysplasia (FD). (*A*) Schematic representation of the transgenic mouse model to express $G\alpha_s$-activating mutations in a tissue-specific manner. (*B*) Quantitative PCR (qPCR) analysis (n = 6) and (*C*) immunoblotting showing elevated expression of $G\alpha_s$ in limb bone from $G\alpha_s^{R201C}$ mice relative to control after doxycycline (Dox) administration. Both intercellular cyclic adenosine monophosphate (cAMP) level (*D*) and protein kinase A (PKA) phosphorylation (*E*) are dramatically elevated in $G\alpha_s^{R201C}$ BMSCs in response of Dox treatment. (*F*) Fluorescence imaging from *Rosa26 mT/mG* reporter mice (mT/mG) shows the expression of Tet-$G\alpha_s$/linker/*Prrx1*-Cre cassette and the initiation of FD (white arrows). White dashed lines outline ossification zone (oz) of growth plate and bone marrow (bm) in control (*Prrx1*-Cre/mT/mG) tissue or unaffected bone marrow (bm) in mutant (Tet-$G\alpha_s$/linker/*Prrx1*-Cre/mT/mG) tissue. The genotype of the mice corresponds to control-A = linker, control-B = linker/*Prrx1*-Cre, control-C = Tet-$G\alpha_s$/linker, $G\alpha_s^{R201C}$ = Tet-$G\alpha_s$/linker/*Prrx1*-Cre. Note: control mice, if not indicated, were selected randomly from mice which did not include the three Tet-$G\alpha_s$/linker/*Prrx1*-Cre transgenes. These terms are also applied for the rest of figure legends. Data are presented as mean ± SD, and significance was calculated by Student's t test ($P > 0.05$; $^*P < 0.05$; and $^{***}P < 0.001$).

$G\alpha_s^{R201C}$ Expression in Postnatal Skeletal Progenitors Arrest Their Osteogenic Terminal Differentiation. FD is characterized histologically by the presence of abundant fibroblast-like cells with pre-osteoblastic characteristics in fibrotic areas. As is typical of FD, the islands of dysplastic, woven bone in lesions are not rimmed by mature osteoblasts (23–25). The fibroblast-like FD cells express early osteogenic markers, as assessed immunohistochemically, including the runt-related transcription factor 2 (Runx2), osterix (Osx), and alkaline phosphatase (Alp) (Fig. 5*A*). However, the late osteogenic marker, osteocalcin (Ocn), was poorly expressed (Fig. 5*A*). In contrast, only the calcified structures and abnormal osteoblasts on the surface of the woven bone showed moderate expression of Ocn. These data support the concept that the FD fibroblastic-like cells are osteogenic precursors and that $G\alpha_s^{R201C}$ impairs osteogenic differentiation of immature osteogenic cells into osteoblasts (27).

To assess the effect of $G\alpha_s^{R201C}$ on osteogenic differentiation, we took advantage of the EE tag to assess by double-labeling immunofluorescence coexpression of $G\alpha_s^{R201C}$ with various markers of osteogenic differentiation. During FD lesion progression, $G\alpha_s^{R201C}$ was highly expressed with early osteogenic markers, as evidenced by colocalization of EE tag with the early osteogenic markers Runx2, Osx, Alp, and Collagen 1 (Col1) (Fig. 5*B*). Again, the mature osteoblast marker, Ocn was rarely observed within FD-like lesions,

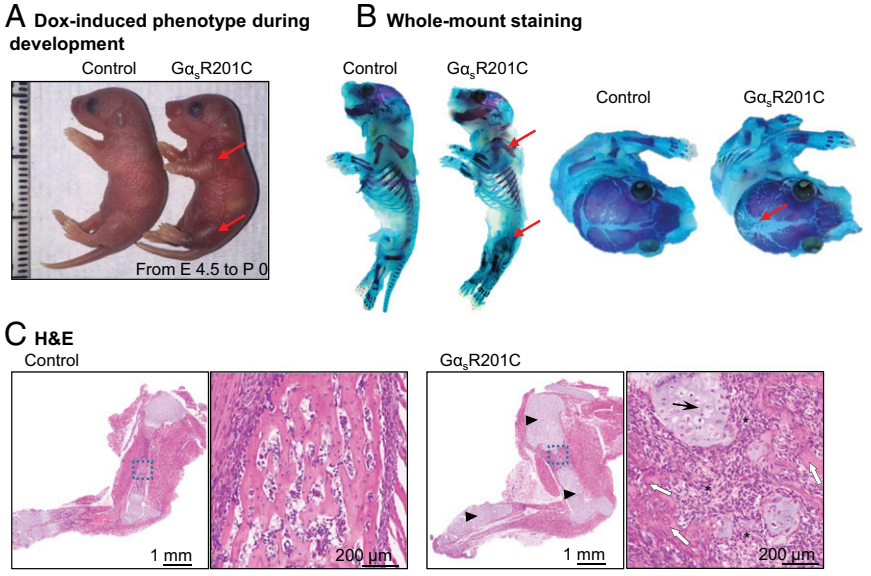

Fig. 2. $G\alpha_s^{R201C}$ expression during embryogenesis results in FD-like lesions. (*A*) Representative image of the expended limbs of $G\alpha_s^{R201C}$ mice (red arrows). (*B*) Whole-mount staining showing the deformity and cortical lytic changes of the limb bone (red arrows) and large nonmineralized areas of the skull in $G\alpha_s^{R201C}$ mice (red arrows). (*C*) H&E sections present limb bone deformity of $G\alpha_s^{R201C}$ mice with predominance of chondroid matrix (arrowheads) and reduced endochondral ossification. In the higher magnification of the blue square of $G\alpha_s^{R201C}$ mice, chondroblasts (black arrows) can be clearly observed, and irregularly shaped woven bone (white arrows) embedded in a fibrocellular matrix (stars) and not rimmed by osteoblasts.

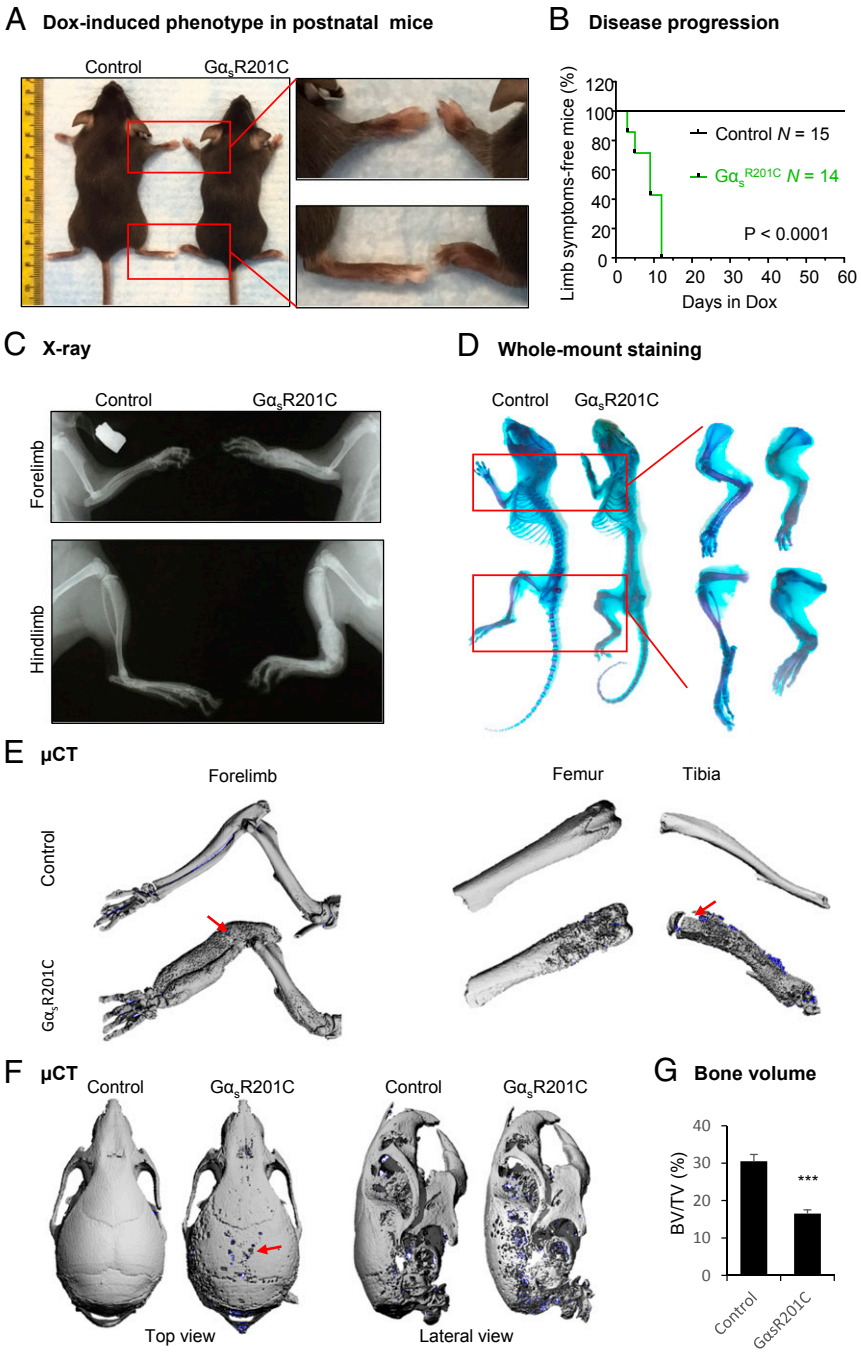

Fig. 3. FD lesions in limbs and skulls of postnatal $G\alpha_s^{R201C}$ mice. (*A*) Representative image of the expanded limbs of adult $G\alpha_s^{R201C}$ mice. (*B*) Kaplan–Meier curve of mice free of visible disease symptoms (limb expansion and limping behavior). $G\alpha_s^{R201C}$ (n = 14) mice developed bone lesions within 14 d after Dox administration. Control (n = 15) mice remained lesion-free. (*C*) X-ray examination shows the expansive deformity of long bones. A mixture of lucent and sclerotic images, representing cortical lytic-sclerotic changes, described as ground glass appearance found in human FD patients. (*D*) Whole-mount staining showing the expansive deformity and lytic changes of the limb bone from $G\alpha_s^{R201C}$ mice. (*E*) μCT examination of limbs showing the lytic-sclerotic lesions with subtle spontaneous fracture (red arrows). (*F*) μCT examination of skulls, showing the lytic defect (red arrow). (*G*) Bone volume (BV) fraction (BV/TV) in the regions of limb with FD lesions (total volume, TV) and the corresponding regions in control mice (n = 4). Data are presented as mean ± SD, and significance was calculated by Student's t test (***P < 0.001).

but was evident in the cells in the mature mineralized bone (Fig. 5*B*). Paralleling the finding of a mineralization defect observed histologically, BMSCs isolated from $G\alpha_s^{R201C}$ mice showed a severe impaired mineralization capacity upon expression of $G\alpha_s^{R201C}$, which induced by Dox (Fig. S4*A*). Furthermore, we observed highly proliferative (27) activity and relatively low apoptotic rates of the fibroblast-liked cells demonstrated by 5-ethynyl-2′-deoxyuridine (EdU) proliferation assay and anti-caspase3 staining, respectively (Fig. 5 *C* and *D*).

Taken together, these findings support the role of skeletal progenitors as FD lesion initiators, in which activating mutations of $G\alpha_s$ promote their proliferation in an expansive, dysregulated fashion. The excess woven bone matrix synthetized by these SSC-derived progenitors may fail to mineralize properly due to an arrested differentiation and abnormal matrix expression.

$G\alpha_s^{R201C}$-Expressing Cells Induce Osteoclastogenesis and Increase Bone Resorption. Human skeletal progenitors harboring $G\alpha_s$ mutants express receptor activator of nuclear factor kappa-B ligand (Rankl), which leads to increased bone resorption of dysplastic bone in FD (28). In a rapid response to Dox administration, differentiation of osteoclasts was significantly stimulated surrounding areas of woven bone in the limbs of $G\alpha_s^{R201C}$ mice, as evidenced by an increased number of tartrate-resistant acid phosphatase (TRAP)-positive multinucleated cells, pointing to increased osteoclastogenesis and bone resorption (Fig. S2*A*). After 2 wk of $G\alpha_s^{R201C}$ induction, numerous resorbing osteoclasts with lacunae were prominent in FD-like lesions (Fig. 6*A*), which is consistent with the lytic areas observed by X-ray imaging and μCT reconstruction (Fig. 3 *C*, *E*, and *F*). Consistently, increased serum level of tartrate-resistant acid phosphatase 5b (TracP 5b) was

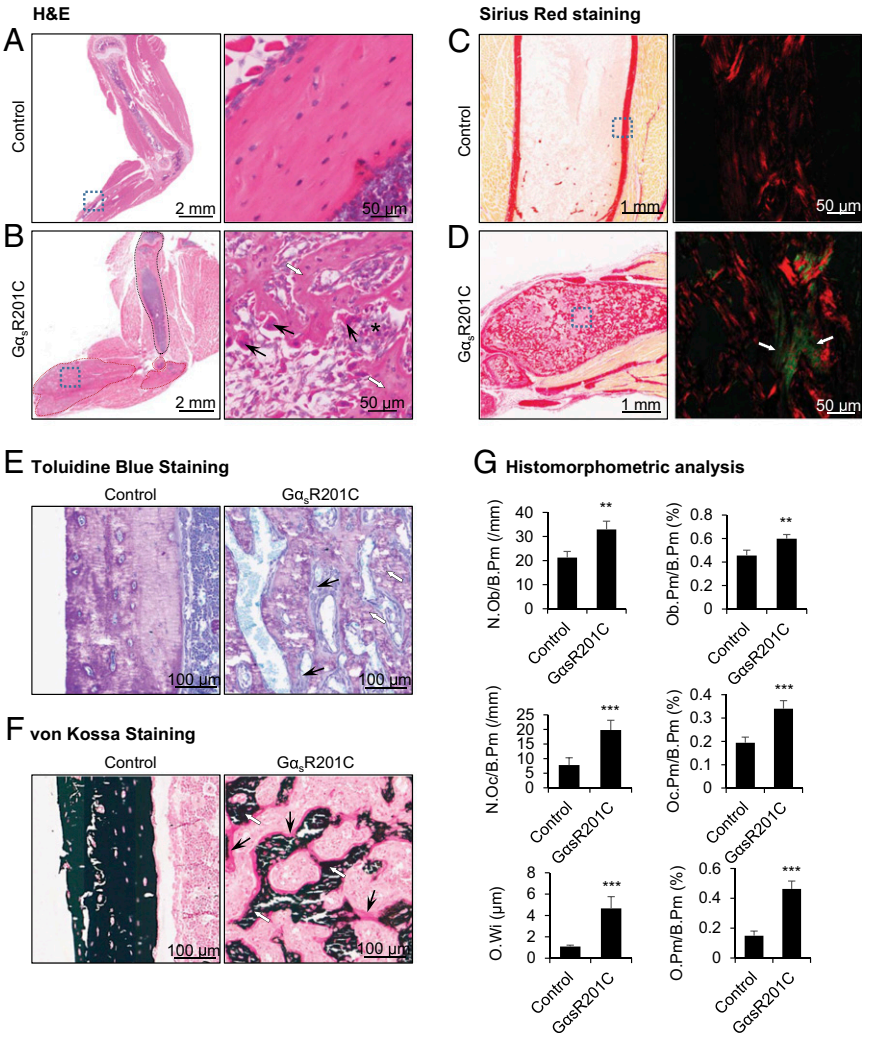

Fig. 4. Histopathological analyses of the FD lesions. (*A*) Normal forelimb bone structure of a control mouse. (*B*) FD bone lesions of a $G\alpha_s^{R201C}$ mouse after Dox administration. *Left* shows a low magnification image of a histological section (H&E), showing a mixture of lighter and dense areas, representing the cystic and fibrotic areas (circled in red) seen in the X-ray, compared with the structure of the unaffected humerus (circled in black). *Right* represents higher magnification of the blue squares at *Left*, to show irregularly shaped trabeculae of immature, undermineralized woven bone (white arrows), embedded in a fibrocellular matrix of soft collagen (stars). The trabeculae are not rimmed by osteoblasts, one of the distinctive features of fibrous dysplasia. The presence of multinucleated giant cells (standard arrows) is evident at this magnification. All these findings highlight similarities with a case of human FD (Fig. S3*A*) with the same legends. (*C* and *D*) Transmitted (*Left*) and polarized light (*Right*) views Sirius Red staining show a widespread disorganized pattern of woven bone in $G\alpha_s^{R201C}$ mice. *Right* represents higher magnification of the blue squares at *Left*, to show green birefringent collagen-rich fibrosis as seen under polarized light. Red color represents bone. Toluidine Blue (*E*) and von Kossa (*F*) staining of undecalcified limb sections show irregular shaped undermineralized woven bone (white arrows), which are surrounded by excess osteoid (black arrows) in $G\alpha_s^{R201C}$ mice. (*G*) Histomorphometric analyses of the regions of limb with FD lesions and the corresponding regions in controls. Bone surface (B.Pm), osteoblast number (N.Ob), osteoblast surface (Ob.Pm), osteoclast number (N.Oc), osteoclast surface (Oc.Pm), osteoid thickness (O.Wi), osteoid surface (O.Pm). $n = 8$ normal and 8 FD tissues sections. Data are presented as mean ± SD, and significance was calculated by Student's *t* test (**$P < 0.01$ and ***$P < 0.001$).

found in $G\alpha_s^{R201C}$ mice (Fig. 6*B*). To explore the mechanism of elevated osteoclast differentiation, we measured the expression of *Rankl* and its decoy receptor, *Osteoprotegerin* (*Opg*) by qPCR analysis. *Rankl* and *Rankl*/*Opg* values were significantly increased in $G\alpha_s^{R201C}$ mice (Fig. 6*C* and Fig. S4*B*). As expected, the circulating level of Rankl was also remarkably elevated in $G\alpha_s^{R201C}$ mice (Fig. 6*D*). The excess Rankl was secreted by FD-initiating $G\alpha_s^{R201C}$ cells, as evidenced by colocalization with EE tag (Fig. 6*E*). The association of Rankl with osteoclasts, indicated by cathepsin K (Ctsk) staining (Fig. 6*F*), further supports the notion that the maturation of osteoclasts was stimulated by Rankl- and *GNAS*-expressing cells within FD-like lesions (29).

Reducing $G\alpha_s^{R201C}$ Expression Results in Clinical Improvement of the Preexisting FD Bone Lesions. To test whether reducing the expression of activated $G\alpha_s$ will result in a regression of the FD-like lesions, Dox administration was discontinued after 2 wk, at a time when FD lesions were readily evident. Mice were followed for an additional 4 mo (Fig. 7*A*). μCT examination revealed mice had slightly thickened limbs of $G\alpha_s^{R201C}$, but without porous-like, lytic phenotype or fractures (Fig. 7*B*). Surprisingly, there were no significant differences in the bone volume between $G\alpha_s^{R201C}$ in control mice at this stage (Fig. 7*C*). As seen on H&E staining, the limbs of $G\alpha_s^{R201C}$ mice exhibited a dramatic recovery, with dense cortical bone and proper enclosed diaphyseal marrow cavity. We noticed that the remineralized cortical bone, recovered from previous widespread fibrous tissue, was fused together, narrowing the marrow cavity compared with littermate controls (Fig. 7*D*). Hematopoietic cells were able to repopulate the marrow spaces at the recovered lesional sites with increased numbers of adipocytes (black arrows and star area) (Fig. 7*D*). Collagen-rich fibrocellular matrix and multinucleated giant cells were not present at this stage. Von Kossa staining of undecalcified limb tissue demonstrated normal mineralization of cortical bone without lesional osteoid in $G\alpha_s^{R201C}$ mice (Fig. 7*E*). Osteoclastic resorption in preexisting FD lesions was dramatically reduced, as demonstrated by minimal TRAP staining (Fig. 7*F*). We also observed significant remineralization in the cranial area as seen on μCT examination. The skull of $G\alpha_s^{R201C}$ mice showed a normal morphology with healed sutures (Fig. 7*G*). The significant clinical improvement of limbs and skulls in mice that were previously affected with FD after the discontinuation of $G\alpha_s^{R201C}$ expression, indicates that stopping the expression or activity of $G\alpha_s^{R201C}$ mutants halts FD progression and may promote the regression of preexisting FD lesions.

Discussion

We have generated a conditional and doxycycline-inducible mouse model for FD and show that the expression in the SSC lineage of $G\alpha_s^{R201C}$ results in a rapid onset of disease exclusively in the skull and long bones, the two most problematic and common areas for FD in humans. By mimicking the manifestations of human FD with this mouse model, we conclusively demonstrate that expression of $G\alpha_s$-activating mutations in skeletal progenitor cells, including its SSC compartment, is sufficient and necessary to establish FD in embryos and adult mice.

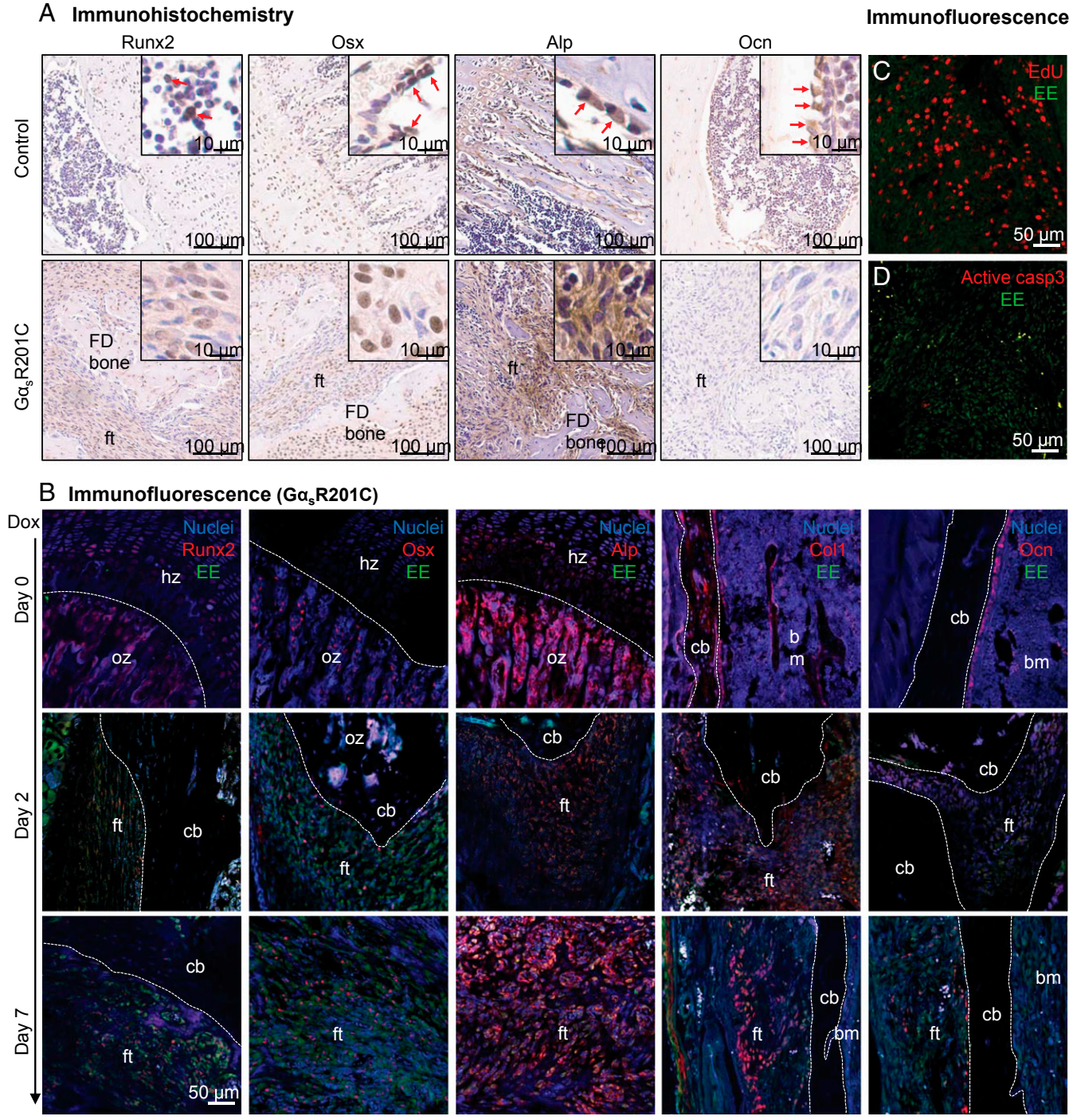

Fig. 5. The preosteogenic feature of $G\alpha_s^{R201C}$ mutant cells. (*A*) Immunohistochemistry of osteogenic markers in control and FD limb bone sections. Runt-related transcription factor 2 (Runx2), osterix (Osx), and alkaline phosphatase (Alp) are enriched in the fibroblastic-like cells within fibrous tissue (ft); Ocn is only found positive in the cells in contact with lesional trabeculae. (*B*) Double-labeling immunofluorescence staining show elevated expression of early osteogenic markers in Glu-Glu (EE) tag-positive $G\alpha_s^{R201C}$ mutant cells along the development of FD. In tissues of day 0, white dashed lines outline boundaries between the hypertrophic zone (hz) and ossification zone (oz) of growth plate or boundaries between cortical bone (cb) and bone marrow (bm); in tissues of day 2 and day 7, white dashed lines outline boundaries between FD lesions (fibrous tissue, ft) and unaffected cortical bone (cb) or bone marrow (bm). Col1; Collagen I. 5-ethynyl-2′-deoxyuridine (EdU) click staining (*C*) and cleaved caspase-3 immunofluorescence staining (*D*) showed high proliferation and relatively low apoptosis rate of $G\alpha_s^{R201C}$ mutant cells.

We first took advantage of the tissue-specific Cre-recombinase expression driven by the *Prrx1* gene to explore the effect of activating mutations of *GNAS* during embryogenesis. Our data show that activating mutations of $G\alpha_s$ in developing cranial and limb bones result in expansive bone deformities and mineralization deficiency, in contrast to the lack of effects of $G\alpha_s^{R201C}$ on embryonic bone development, which was reported previously (16). Instead, we demonstrated that $G\alpha_s^{R201C}$ mutations are sufficient to induce typical FD phenotype when expressed in skeletal progenitors. In the current study, significant bone defects were mainly

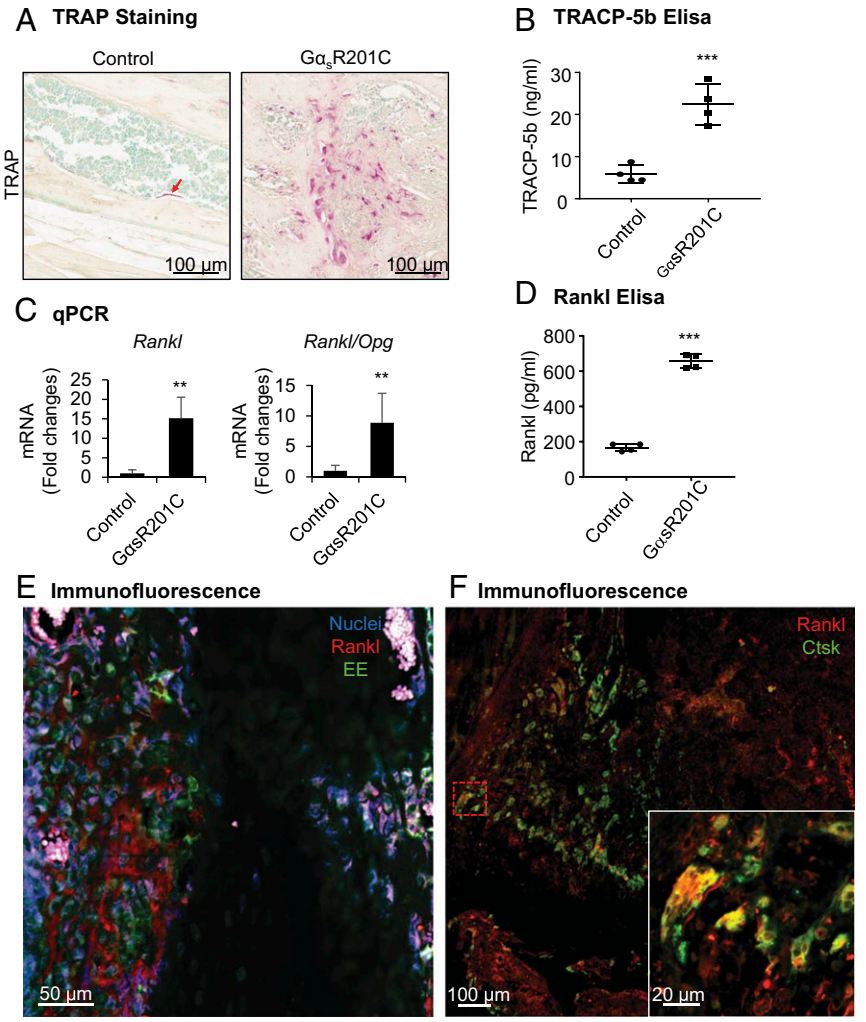

Fig. 6. $G\alpha_s^{R201C}$ leads to increased bone resorption via the Rankl pathway. (*A*) Tartrate-resistant acid phosphatase (TRAP) staining of limb bone indicates the presence of numerous osteoclasts in $G\alpha_s^{R201C}$ mice ($n = 4$). (*B*) Serum level of tartrate-resistant acid phosphatase 5b (TracP 5b) was elevated in $G\alpha_s^{R201C}$ mice ($n = 4$). Scatterplots are plus mean (*Middle* line). (*C*) qPCR analysis shows significantly increased *Rankl* and *Rankl/Opg* ratio ($n = 6$). (*D*) Serum level of Rankl was significantly increased in $G\alpha_s^{R201C}$ mice ($n = 4$). Scatterplots are plus mean (*Middle* line). (*E*) Immunofluorescence staining shows colocalization of Rankl with EE tag in fibroblastic-like cells expressing $G\alpha_s^{R201C}$. (*F*) Immunofluorescence staining shows binding of Rankl with osteoclasts, which are marked by cathepsin K (Ctsk). Opg, osteoprotegerin; Rankl, receptor activator of nuclear factor kappa-B ligand. Data are presented as mean ± SD, and significance was calculated by Student's *t* test (**$P < 0.01$ and ***$P < 0.001$).

observed in calvarial sutures and bones in $G\alpha_s^{R201C}$ mice (Figs. 2*B* and 3*F*). However, we did not observe significant pathological changes in bones of the skull base, which is consistent with others' finding that postnatal calvarial SSCs expressing *Prrx1* reside exclusively in calvarial sutures (21). Further efforts will be devoted to the detailed analysis of FD progression and pathological manifestations in the cranial area. These data lend support to the hypothesis that a subset of embryonic bone progenitor cells may already harbor the causative mutation of FD (6). This in turn raises the possibility that FD initiating cells promoting subclinical lesions may already be present at birth, which undetected, may then progress to FD/MAS during childhood.

At the cellular level, our data suggest that $G\alpha_s^{R201C}$-initiated FD development involves several distinct mechanisms. As depicted in Fig. S5, initially $G\alpha_s^{R201C}$ expression accelerates the proliferation of skeletal progenitor cells, including skeletal stem cells, which remain committed to early stage osteogenic lineage, as judged by the expression of Runx2, Osx, Alp, and Col1, typical of preosteoblastic cells. However, these cells cannot undergo full differentiation from preosteoblasts to mature osteoblasts. This is accompanied by impaired mineralization (30, 31) as well as robust expression and secretion of Rankl by these preosteoblastic cells that stimulate abundant osteoclastogenesis and bone resorption. Indeed, the combined overgrowth of fibroblast-like, poorly differentiated preosteoblasts, with the remarkable activation of osteoclasts and bone remodeling by $G\alpha_s^{R201C}$-expressing cells may underlie the rapid formation of FD lesions upon expression of $G\alpha_s^{R201C}$ in SSC lineage.

To date, there is no cure for FD. The available medical treatments are only palliative, focusing on relieving symptoms. The frequent pathological fractures and pain that accompany FD may be related to abundant osteoclastic bone resorption. The palliative effect of antiresorptive agents such as bisphosphonates (32) and denosumab (human monoclonal Rankl antibody) (33) is consistent with this observation. However, their efficacy is limited and is not sufficient to abrogate the progression of the FD or to decrease fractures (34, 35). Our data suggest that reducing the expression or signaling capacity of activating mutations of $G\alpha_s^{R201C}$ can halt the progression of the FD, promote the regression of preexisting FD lesions, and by subsequent remodeling, perhaps even improve skeletal architecture. These data further confirm the causal relationship between $G\alpha_s^{R201C}$ and

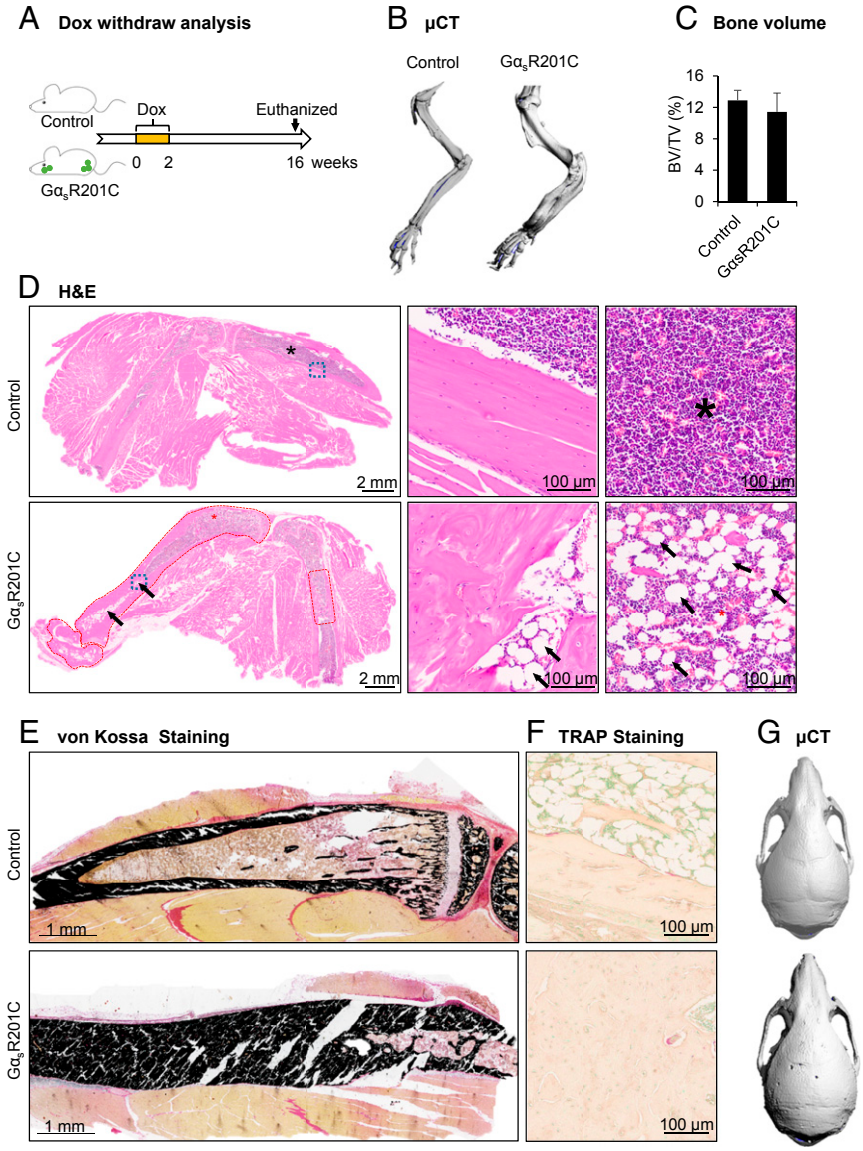

Fig. 7. Reducing *GNAS* expression following Dox withdrawal results in clinical improvement of the preexisting FD bone lesions. (*A*) Schematic representation of the Dox treatment of control and $G\alpha_s^{R201C}$ mice. (*B*) μCT examination showed the slightly thickened limb bone of the $G\alpha_s^{R201C}$ mice without porous-like lytic phenotype or fracture. (*C*) No significant difference of bone volume fraction between control and $G\alpha_s^{R201C}$ mice ($n = 4$). (*D*) H&E section of both control and $G\alpha_s^{R201C}$ mouse. The preexisting FD lesions circled in red exhibit a dramatic recovery, dense cortical bone with disordered trabecular processes. The diaphyseal marrow cavity exhibits clear boundaries, although slightly narrower than in littermate control, and are composed of hematopoietic cells and adipocytes (black arrows). Details can be better viewed in the *Middle* and *Right* which represent higher magnification of the blue squares and stars area in *Left*, respectively. Note the collagen-rich fibrocellular matrix and multinucleated giant cells are not present at this stage. (*E*) Von Kossa staining of undecalcified limb tissue shows normal mineralization of cortical bone without lesional osteoid in $G\alpha_s^{R201C}$ mice. (*F*) TRAP staining shows dramatically reduced number of osteoclasts in remineralized bone 16 wk after discontinuing Dox (compare with Fig. 6*A*). (*G*) μCT examination of the recovery skull of $G\alpha_s^{R201C}$ mice compared with its littermate. Data are presented as mean ± SD, and significance was calculated by Student's *t* test. No significant differences were observed.

FD and establish the strict dependence of FD on persistent $G\alpha_s^{R201C}$ activity to support the maintenance of FD lesions.

Together, the data lend support to the hypothesis that a cure for FD could be brought about by reducing the expression of $G\alpha_s^{R201C}$ and/or its associated downstream molecular events. Regarding the latter, we observed a remarkable activation of PKA upon mutant $G\alpha_s^{R201C}$ expression in BMSCs. In turn, we can postulate that PKA-regulated transcriptional events may promote the expression of the Rankl promoter, similar to that induced by PTH or 1,25 dihydroxyvitamin D3 [1,25(OH) 2D3] (36). However, why PKA stimulation may halt the terminal differentiation of osteoblastic precursors is still unknown. While detailed analysis of transcriptional programs elicited in vivo by $G\alpha_s^{R201C}$ can now be explored in our animal model, recent findings supporting that PKA can control histone modification marks (37, 38) may provide new avenues in the search of a treatment for FD. Specifically, our recent study revealing that PKA controls stem cell fate in the skin (17) and recent evidence that PKA activation promotes epigenetic gene repression by histone H3 with acetylated lysine 9 (H3K9) demethylation, suggests that many new cancer therapies targeting epigenetic mark writers, readers, or erasers can now be deployed for FD therapy. In addition, recent high-throughput small molecule library screens have identified multiple novel drug candidates, however, their evaluation for FD/MAS treatment has been hampered by the dearth of suitable animal models of this disease (39). In this regard, several

of the features of our mouse model, specifically rapid onset of phenotype with appropriate histological FD manifestations, and the reversion of FD lesions after blocking pathologic $G\alpha_s^{R201C}$ expression, may represent an ideal platform to discover precision treatment approaches disrupting $G\alpha_s^{R201C}$-driven growth, and/or restoring normal skeletal stem cell differentiating circuitries in FD.

Materials and Methods

Generation of $G\alpha_s^{R201C}$ Mice. The disease model mice are triple transgenic mice obtained by breeding a strain that express Cre driven by the *Prrx1*-derived enhancer [B6.Cg-Tg(Prrx1-cre)1Cjt/J, referred to as "*Prrx1*-Cre" mice], with ROSA26-LSL-rtTA-IRES-GFP mice able to express reverse tetracycline transactivator and GFP after Cre recombination [B6.Cg-Gt(ROSA)26Sortm1(rtTA, EGFP)Nagy/J, referred to as linker mice], with mice carrying the mutated human *GNAS*^{R201C} gene and bearing a long internal EE tag, described previously (17) (referred to as "Tet-$G\alpha_s$" mice). To demonstrate sites of Cre recombination, the $G\alpha_s^{R201C}$ mice were bred with double-fluorescent Cre reporter mice (*Rosa26 mT/mG*). All mice except Tet-$G\alpha_s$ mice were obtained from The Jackson Laboratory.

All mice were of mixed background between C57BL/6 and FVB/N. All animal studies were carried out according to NIH Intramural Animal Care and Use Committee-approved protocols and the University of California San Diego (UCSD) Institutional Animal Care and Use Committee-approved protocols, in compliance with the Guide for the Care and Use of Laboratory Animals. Both male and female mice were used in the studies, if not specified. All experiments were conducted using littermate controls. In the tetracycline-inducible mice, doxycycline (Dox) (Sigma-Aldrich) was administered either in a concentration ranging from 0.01 to 1 g/L in drinking water or 6 g/kg in the diet (Newco specialty division). Treatment was started between embryonic day 4.5 and 2 wk after birth, for up to 2 consecutive weeks, as indicated in each experimental group.

Tissue Collection and Processing. Fresh bone tissues were frozen in dry ice immediately after collection and homogenized. Bone tissue samples were collected and fixed in zinc 10% formalin buffered fixative solution at room temperature overnight and then stored in 70% ethanol for further embedding. Fixed skeletal samples were either decalcified in 4% buffered EDTA for paraffin and optimal cutting temperature (OCT) frozen embedding or embedded in PMMA (40) without decalcification. H&E staining sections were obtained from paraffin sections for further histological assessment. Please see *SI Extended Materials and Methods* for additional details.

X-Ray, Microcomputed Tomography. Radiograms were taken using a Faxitron MX-20 Specimen Radiography System and microcomputed tomography (μCT) analysis was performed according to the standard guidelines (41) using a SCANCO Medical μCT 40 system (SCANCO Medical). We also assessed the bone volume fraction (BV/TV) in the regions of limb with FD lesions and the corresponding regions in controls. Please see *SI Extended Materials and Methods* for additional details.

Whole-Mount Skeletal Staining (Alizarin Red and Alcian Blue Staining). Mice were killed, skinned, and eviscerated, and then fixed in 100% ethanol overnight. The specimens were then immerged in staining solution for 3 d and processed according to standard protocols for Alizarin Red S (ARS) staining. Please see *SI Extended Materials and Methods* for additional details.

Sirius Red Staining. Paraffin-embedded tissue sections were deparaffinized and stained in Picro-Sirius Red solution, counterstained with methyl green (Vector), dehydrated, and evaluated under both transmitted light and polarized light microscopy. Please see *SI Extended Materials and Methods* for additional details.

TRAP Staining. Sections were incubated at 37 °C in freshly prepared TRAP staining solution, rinsed in distilled water, counterstained with methyl green (Vector), dehydrated, and mounted. Please see *SI Extended Materials and Methods* for additional details.

Bone Histomorphometric Analyses. Bone histomorphometric measurements were performed on undecalcified PMMA-embedded bone sections after Toluidine Blue and von Kossa/nuclear fast red staining, using OsteoMeasure software (OsteoMetrics). The region of interest excluded the area within 0.25 mm from the growth plate. All histomorphometric parameters were calculated and expressed according to the suggestions made by the American Society for Bone and Mineral Research nomenclature committee (42).

RNA Isolation and qRT-PCR. Total RNA was isolated from both bone tissues and cells using the TRIzol reagent (Invitrogen) according to the manufacturer's instructions. Reverse transcription was performed followed by qRT-PCR analysis using iQ SYBR Green Supermix (Bio-Rad) on a Bio-Rad iCycler iQ multicolor real-time PCR detection system. Target gene expression levels were normalized with *Gapdh*. Please see *SI Extended Materials and Methods* for additional details and oligonucleotides used for amplification.

Immunoblot Analysis. Western blot assays were performed and repeated at least three times as previously described (17). Please see *SI Extended Materials and Methods* for additional details and all antibodies used.

Immunohistochemistry and Immunofluorescence. For immunohistochemistry, paraffin sections were deparaffinized and rehydrated, endogenous peroxide activity was blocked using 3% hydrogen peroxide, and heat-mediated antigen retrieval was performed. The sections were blocked with 10% FBS (Gibco) in PBS for 1 h then incubated with primary antibodies overnight at 4 °C, followed by incubation of biotinylated secondary antibodies for 30 min at room temperature. Sections were detected using ABC and DAB systems, and then counterstained with hematoxylin. The slides were scanned using an Aperio AT2 Slide Scanner. For double-labeling immunofluorescence, the OCT-embedded frozen sections were blocked and incubated with primary antibodies overnight as were the paraffin sections. Sections were then incubated for 30 min with Alexa Fluor-conjugated secondary antibodies, followed by nuclei staining with Hoechst 33342 for 15 min at room temperature. The slides were mounted and images were acquired and analyzed using a confocal microscope, as described below. Please see *SI Extended Materials and Methods* for additional details and the antibodies used. Each immunostaining was repeated in at least three independent mice or three independent experiments; multiple fields were reviewed.

Fluorescent Imaging. Confocal fluorescent images were used to analyze the double-labeling immunofluorescence staining in both control and FD tissues. Please see *SI Extended Materials and Methods* for additional details.

EdU Proliferation Assay. The proliferation assay was performed as previously described (43). Briefly, 100 μL of 10 mM EdU per 10 g of mouse body weight was administered 3 h before killing, before proceeding to decalcification and sectioning. The click staining and the following immunofluorescence staining were performed according to the manufacturer's instructions (Invitrogen, Click-iT EdU Alexa Fluor 647 Imaging Kit).

Bone Marrow Stromal Cell Culture and Osteogenic Induction. Primary mouse BMSCs were isolated and cultured as previously described (44). The osteogenic differentiation induction was performed as previously described (45). To characterize the osteoblastic phenotypes, ARS staining was performed to assess the mineralization of extracellular matrix after 14 d of osteogenic induction. Cells were rinsed with PBS and fixed in 4% paraformaldehyde for 1 h at room temperature. After washing with PBS, cells were stained with freshly made ARS staining solution and then washed in distilled water. Please see *SI Extended Materials and Methods* for additional details.

ELISA. For cAMP ELISA, BMSCs were seeded in 24-well plates at a density of 1×10^5 cells per well and incubated overnight in serum-free medium. Then cells were incubated in the presence of 5 μg/mL Dox for 2 h. The phosphodiesterase inhibitor, 0.2 mM 3-isobutyl-1-methylxanthine (IBMX) (Sigma-Aldrich) was added to the medium 30 min before harvest. Intracellular cAMP levels were measured using the Mouse/Rat cAMP Parameter Assay Kit (R&D systems). For tartrate-resistant acid phosphatase 5b (TRACP 5b) and TNF-related activation-induced cytokine (TRANCE, RankI) ELISA, mice were killed for serum collection. Serum samples were then analyzed by ELISA according to manufacturer's instructions. Please see *SI Extended Materials and Methods* for additional details.

Statistical Analysis. Statistical analyses were from at least triplicate experiments. Unpaired *t* test or ANOVA were used to evaluate significance in two or more than two sample groups, respectively. All analyses were carried out using Prism 6 statistical analysis program (GraphPad). Statistical significance was reported as follows: NS for not significant or $P > 0.05$; $^*P < 0.05$; $^{**}P < 0.01$; and $^{***}P < 0.001$. All data are reported as mean ± SD.

ACKNOWLEDGMENTS. We thank Dr. Zbigniew Mikulski for the whole-tissue fluorescent imaging. This project was supported by 111 Project Grant B14038 from the Ministry of Education of China; National Natural Science Foundation of China Grants 81520108009, 81621062, 81722014, 81671024,

81371171, and 81571009; University of Pennsylvania Orphan Disease Center, with support from the Fibrous Dysplasia Foundation; funding from the University of California, San Diego (UCSD) Department of Pharmacology and Moores Cancer Center; and the Division of Intramural Research, National Institute of Dental and Craniofacial Research, National Institutes of Health. D.J.S. was supported in part by the UCSD Graduate Training Program in Cellular and Molecular Pharmacology through National Institute of General Medical Sciences Institutional Training Grant T32 GM007752.

1. Weinstein LS, et al. (1991) Activating mutations of the stimulatory G protein in the McCune-Albright syndrome. *N Engl J Med* 325:1688–1695.
2. Leet AI, Collins MT (2007) Current approach to fibrous dysplasia of bone and McCune-Albright syndrome. *J Child Orthop* 1:3–17.
3. Turan S, Bastepe M (2015) GNAS spectrum of disorders. *Curr Osteoporos Rep* 13: 146–158.
4. Bianco P, et al. (1998) Reproduction of human fibrous dysplasia of bone in immunocompromised mice by transplanted mosaics of normal and Gsalpha-mutated skeletal progenitor cells. *J Clin Invest* 101:1737–1744.
5. Bianco P, Robey P (1999) Diseases of bone and the stromal cell lineage. *J Bone Miner Res* 14:336–341.
6. Riminucci M, Saggio I, Robey PG, Bianco P (2006) Fibrous dysplasia as a stem cell disease. *J Bone Miner Res* 21(Suppl 2):P125–P131.
7. Riminucci M, Robey PG, Saggio I, Bianco P (2010) Skeletal progenitors and the GNAS gene: Fibrous dysplasia of bone read through stem cells. *J Mol Endocrinol* 45:355–364.
8. Shenker A, et al. (1993) Severe endocrine and nonendocrine manifestations of the McCune-Albright syndrome associated with activating mutations of stimulatory G protein GS. *J Pediatr* 123:509–518.
9. Gorham LW, Campbell EH, Howard WC, Donhauser JL, Rust NH (1941) Albright's syndrome-A group of cases characterized by osteitis fibrosa disseminata, areas of pigmentation and a gonadal dysfunction. *Trans Am Clin Climatol Assoc* 57:179–187.
10. Weinstein LS, Liu J, Sakamoto A, Xie T, Chen M (2004) Minireview: GNAS: Normal and abnormal functions. *Endocrinology* 145:5459–5464.
11. Pivonello R, et al. (2015) Neuropsychiatric disorders in Cushing's syndrome. *Front Neurosci* 9:129.
12. Collins MT, Singer FR, Eugster E (2012) McCune-Albright syndrome and the extraskeletal manifestations of fibrous dysplasia. *Orphanet J Rare Dis* 7(Suppl 1):S4.
13. O'Hayre M, et al. (2013) The emerging mutational landscape of G proteins and G-protein-coupled receptors in cancer. *Nat Rev Cancer* 13:412–424.
14. DiCaprio MR, Enneking WF (2005) Fibrous dysplasia. Pathophysiology, evaluation, and treatment. *J Bone Joint Surg Am* 87:1848–1864.
15. Carter JM, et al. (2014) Activating GNAS mutations in parosteal osteosarcoma. *Am J Surg Pathol* 38:402–409.
16. Saggio I, et al. (2014) Constitutive expression of Gsalpha(R201C) in mice produces a heritable, direct replica of human fibrous dysplasia bone pathology and demonstrates its natural history. *J Bone Miner Res* 29:2357–2368.
17. Iglesias-Bartolome R, et al. (2015) Inactivation of a Gα(s)-PKA tumour suppressor pathway in skin stem cells initiates basal-cell carcinogenesis. *Nat Cell Biol* 17:793–803.
18. Logan M, et al. (2002) Expression of Cre recombinase in the developing mouse limb bud driven by a Prxl enhancer. *Genesis* 33:77–80.
19. Regard JB, et al. (2013) Activation of hedgehog signaling by loss of GNAS causes heterotopic ossification. *Nat Med* 19:1505–1512.
20. Kawanami A, Matsushita T, Chan YY, Murakami S (2009) Mice expressing GFP and CreER in osteochondro progenitor cells in the periosteum. *Biochem Biophys Res Commun* 386:477–482.
21. Wilk K, et al. (2017) Postnatal calvarial skeletal stem cells expressing PRX1 reside exclusively in the calvarial sutures and are required for bone regeneration. *Stem Cell Reports* 8:933–946.
22. Belteki G, et al. (2005) Conditional and inducible transgene expression in mice through the combinatorial use of Cre-mediated recombination and tetracycline induction. *Nucleic Acids Res* 33:e51.
23. Riminucci M, et al. (1997) Fibrous dysplasia of bone in the McCune-Albright syndrome: Abnormalities in bone formation. *Am J Pathol* 151:1587–1600.
24. Toyosawa S, et al. (2007) Ossifying fibroma vs fibrous dysplasia of the jaw: Molecular and immunological characterization. *Mod Pathol* 20:389–396.
25. Riminucci M (2003) FGF-23 in fibrous dysplasia of bone and its relationship to renal phosphate wasting. *J Clin Invest* 112:683–692.
26. Ippolito E, et al.; European Pediatric Orthopaedic Society (2003) Natural history and treatment of fibrous dysplasia of bone: A multicenter clinicopathologic study promoted by the European Pediatric Orthopaedic Society. *J Pediatr Orthop B* 12:155–177.
27. Shenker A, Weinstein LS, Sweet DE, Spiegel AM (1994) An activating Gs alpha mutation is present in fibrous dysplasia of bone in the McCune-Albright syndrome. *J Clin Endocrinol Metab* 79:750–755.
28. Piersanti S, et al. (2010) Transfer, analysis, and reversion of the fibrous dysplasia cellular phenotype in human skeletal progenitors. *J Bone Miner Res* 25:1103–1116.
29. Kondo H, Guo J, Bringhurst FR (2002) Cyclic adenosine monophosphate/protein kinase A mediates parathyroid hormone/parathyroid hormone-related protein receptor regulation of osteoclastogenesis and expression of RANKL and osteoprotegerin mRNAs by marrow stromal cells. *J Bone Miner Res* 17:1667–1679.
30. Regard JB, et al. (2011) Wnt/β-catenin signaling is differentially regulated by Gα proteins and contributes to fibrous dysplasia. *Proc Natl Acad Sci USA* 108: 20101–20106.
31. Wu JY, et al. (2011) Gsα enhances commitment of mesenchymal progenitors to the osteoblast lineage but restrains osteoblast differentiation in mice. *J Clin Invest* 121: 3492–3504.
32. Chapurlat RD (2006) Medical therapy in adults with fibrous dysplasia of bone. *J Bone Miner Res* 21(Suppl 2):P114–P119.
33. Boyce AM, et al. (2012) Denosumab treatment for fibrous dysplasia. *J Bone Miner Res* 27:1462–1470.
34. Mansoori LS, Catel CP, Rothman MS (2010) Bisphosphonate treatment in polyostotic fibrous dysplasia of the cranium: Case report and literature review. *Endocr Pract* 16: 851–854.
35. Chapurlat R (2012) Denosumab in a child with fibrous dysplasia of bone: Too much of a good thing. *IBMS BoneKEy* 9.
36. O'Brien CA (2010) Control of RANKL gene expression. *Bone* 46:911–919.
37. Yamamizu K, et al. (2012) Protein kinase A determines timing of early differentiation through epigenetic regulation with G9a. *Cell Stem Cell* 10:759–770.
38. Pattabiraman DR, et al. (2016) Activation of PKA leads to mesenchymal-to-epithelial transition and loss of tumor-initiating ability. *Science* 351:aad3680.
39. Bhattacharyya N, et al. (2014) A high throughput screening assay system for the identification of small molecule inhibitors of gsp. *PLoS One* 9:e90766.
40. Yuan Q, et al. (2014) Increased osteopontin contributes to inhibition of bone mineralization in FGF23-deficient mice. *J Bone Miner Res* 29:693–704.
41. Bouxsein ML, et al. (2010) Guidelines for assessment of bone microstructure in rodents using micro-computed tomography. *J Bone Miner Res* 25:1468–1486.
42. Dempster DW, et al. (2013) Standardized nomenclature, symbols, and units for bone histomorphometry: A 2012 update of the report of the ASBMR histomorphometry nomenclature committee. *J Bone Miner Res* 28:2–17.
43. Mead TJ, Lefebvre V (2014) Proliferation assays (BrdU and EdU) on skeletal tissue sections. *Methods Mol Biol* 1130:233–243.
44. Nemeth K, Mayer B, Sworder BJ, Kuznetsov SA, Mezey E (2013) A practical guide to culturing mouse and human bone marrow stromal cells. *Curr Protoc Immunol* 102: Unit 22F.12.
45. Zhao X, et al. (2016) Cysteine dioxygenase type 1 inhibits osteogenesis by regulating Wnt signaling in primary mouse bone marrow stromal cells. *Sci Rep* 6:19296.